Asian Journal of Chemistry; Vol. 37, No. 6 (2025), 1385-1391

ASIAN JOURNAL OF CHEMISTRY

https://doi.org/10.14233/ajchem.2025.33732

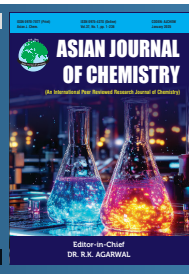

High-Performance Porous Carbon Electrodes from Tea Residues: A Sustainable Approach for Advanced Supercapacitors

C. RAJASEKAR[1], P. KURINJI NATHAN[2], M. ROSELIN RANJITHA[3], S. RAGHU[4,*] and R.A. KALAIVANI[1,*]

[1]Department of Chemistry, Vels Institute of Science, Technology & Advanced Studies (VISTAS), Chennai-600117, India
[2]Department of Physics, PSG College of Arts & Science, Coimbatore-641014, India
[3]Department of Chemistry, Stella Maris College (Autonomous) Affiliated to University of Madras, Chennai-600086, India
[4]Centre for Advanced Research and Development (CARD)/Chemistry, Vels Institute of Science, Technology & Advanced Studies (VISTAS), Chennai-600117, India

*Corresponding authors: E-mail: subraghu_0612@yahoo.co.in; rakvani@yahoo.co.in

Received: 14 March 2025; *Accepted*: 3 May 2025; *Published online*: 27 May 2025; AJC-22012

Carbon electrodes sourced through biomass for application in supercapacitors are currently a significant focus in the development of energy storage devices that prioritize efficiency, environmental sustainability and cost-effectiveness. This investigation highlights a potential avenue for tea residues, concentrating on the conversion of waste to useful resources. Tea residues served as a raw material to produce activated carbon *via* a simple single-step process, aimed at creating highly efficient electrode material for supercapacitors. The samples were subjected to chemical activation using $ZnCl_2$ at two different temperatures (800 and 900 °C). Surface area of the two TRAC samples were analyzed using BET technique and noted as 940.14 m^2/g and 1158.06 m^2/g. The electrochemical investigation was specifically carried out in both aqueous (6 M KOH) and non-aqueous ($TEABF_4$) environments. The TRAC 900 electrode exhibited an impressive specific capacitance of 395.42 F g^{-1} at 1 A g^{-1} and displayed exceptional cycling stability, maintaining 96.66% of its capacitance after 16,000 cycles in a non-aqueous environment. Furthermore, the peak power density attained was around 63,000 W kg^{-1} at an energy density of 35 Wh g^{-1} when subjected to a higher current density of 10 A g^{-1}. The impressive electrochemical performance suggests that the highly ordered porous carbon electrodes derived from used-tea solid waste represent a promising option for high-performance supercapacitors and exemplify the idea of converting waste into valuable resources.

Keywords: Tea residue, Activated carbon, Supercapacitors, Carbon electrodes.

INTRODUCTION

The commercial expectation for hybrid electrical devices and corresponding power storage devices are witnessing significant expansion, leading to an immediate demand for the sophisticated electrochemical energy storage systems [1,2]. The reduction of fossil fuels results in considerable environmental effects that negatively influence the well-being of living organisms [3]. This demand drives the progress of complementary green energy solutions utilizing solar, wind, biomass and a range of other renewable resources [4]. Effective energy storage systems are crucial for capturing and delivering energy generated from these sources. Electrochemical energy storage devices such as batteries, fuel cells and supercapacitors are competing against each other while they offer unique benefits and drawbacks [5]. The storage mechanisms of batteries present certain limitations leading to shortcomings in both energy and power density.

Supercapacitors are considered strong candidates for energy storage due to their impressive stability, long life-cycle performance, high power density, sufficient energy density and eco-friendly attributes [6]. The interaction which happens between the electrode and electrolyte plays a crucial role in the energy storage process. From a mechanistic viewpoint, swift redox processes that involve charge transfer at the interfaces of electrodes and electrolytes dictate the energy storage capacity in pseudo-capacitors. In electrical double-layer capacitors (EDLC), the charges accumulate due to the interaction between oppositely charged ions at the interface layers of the electrode and electrolyte [7]. The materials employed for pseudo capacitor

electrodes often present several significant drawbacks, such as insufficient cycling stability, poor electrical conductivity and high costs, which considerably impede their practical application [8]. In contrast, EDLCs demonstrate elevated power density, impressive stability and notable rate performance [9]. Carbon-based materials are frequently employed as electrode materials in EDLCs due to their chemical stability, conductivity and ecological friendliness [10]. In recent years, various carbon materials [11-15] such as graphene, carbon nanotubes, graphene oxides, carbon aerogels, carbon fibers, *etc*. have been synthesized in the laboratory through innovative methods and applied in supercapacitors.

Nevertheless, the procedure of laboratory synthesis becomes a more complex and expensive undertaking. Consequently, it is crucial to determine an effective strategy for reducing costs. Activated carbons derived from biomass materials often display distinctive structures that are difficult to reproduce through synthetic methods [16]. Recent reports indicate that carbon derived from biomass is becoming the leading supercapacitor electrode material due to its unique structures that are difficult to synthesize artificially [17]. So far, a range of biomass carbon sources, such as corn husk [18], banana peel [19], rice husk [20] and pinecone [21], have been examined for their accessibility and economic viability. Tea waste, a prevalent byproduct produced daily following extraction globally, is often discarded immediately. The composition of the residue includes cellulose, structural proteins, lignin, hemicellulose, minerals and secondary metabolites [22]. The previously mentioned character-istics highlight the considerable potential of tea waste as a carbon precursor in the development of high-performance electrode materials.

This study introduces an activated carbon that demonstrates outstanding supercapacitor performance, created from tea residues to act as precursor for carbon. The synthesized carbon demonstrates remarkable electrical conductivity and excellent wettability, greatly improving the rate performance and durability of cycling. This method facilitates the acquisition of high-quality activated carbons appropriate for supercapacitors and offers an opportunity for the effective use of waste residues produced from daily activities.

EXPERIMENTAL

The tea residues (TRs) were collected from a local tea shop and several residential neighborhoods in Chennai, India. Zinc chloride, Teflon solution (60%), conducting carbon (super P), potassium hydroxide (99 %, KOH), tetraethylammonium tetrafluoroborate (99% $TEABF_4$) and acetonitrile were sourced from Sigma-Aldrich, USA. In this work, all the experiments employed analytical grade chemicals in their original form, without undergoing any further purification processes.

Preparation of nanostructured activated carbon (AC) from tea residues (TRs): The collected tea residues were subjected to an extensive washing procedure using deionized water to remove any remaining traces of milk. The sample underwent drying in an oven set to 60 ºC for 24 h, followed by grinding with a mortar and pestle. Subsequently, the cleaned TRs were amalgamated with $ZnCl_2$ the activating agent in 1:4 mass ratio and ground till it forms a uniform mixture. This mixture was then subjected to dehydrate in an oven maintained at 60 ºC for 24 h to remove moisture. Subsequently, carbonization was performed at 800 and 900 ºC for 6 h, utilizing a constant 5 ºC/min heating rate within a nitrogen tube furnace [23]. After the cooling process, the carbonization products were subjected to removal of impurities and washing procedure with deionized water and 5 wt.% HCl till a neutral pH was reached. Finally, they were dried and referred to as TRAC 800 and TRAC 900.

Preparation of TRAC 900 electrode and cell fabrication: Symmetric supercapacitor test cells were fabricated in a CR2032 coin cell format, employing TRAC 900 as the selected electrode materials. The experimental slurry is developed by mixing tea residue carbon with Teflon binder and carbon black in a weight ratio of 85:5:10, utilizing isopropyl alcohol as solvent. An aluminium foil with a thickness of 20 µm, functioning as a current collector was employed and the slurry was evenly applied onto the foil with a brush. The foil was then dried overnight in vacuum at 80 ºC. In the next stage, a pressure of 10 kg/cm^2 was applied with a hydraulic press to guarantee complete adhesion of the coated slurry on the surface of aluminum current collector. Following this, two discs with a diameter of 1.6 cm were punched out and weighed separately to ascertain the total mass of the materials on each current collector. The coated current collector is held in a vacuum oven maintained under 80 ºC for 6 h, a step performed before the fabrication of coin cells.

To eliminate air throughout the procedure, the cell was constructed in an argon-filled glove box. The "can" and "cap," the two parts of the CR2032 coin cell, are both composed of stainless steel. Two components were kept apart by polypropylene "O" rings that were fastened to the top. The cell measures 2.5 mm in thickness and 20 mm in diameter. The two electrodes of the same weight were separated using a polypropylene carbonate cloth separator. This can now be fixed in a CR2032-type coin cell with either an aqueous electrolyte of 6M KOH or an organic electrolyte, 1M $TEABF_4$ in acetonitrile. To increase the wettability of the electrode surface, the cell was evacuated prior to the electrolyte being injected to remove any excess air or oxygen. Supercapacitor coin cells were then created by crimp-sealing the entire device in a fly press. The specific capacitance (C), power density (P) and energy density (E) were determined using the eqns. 1-3 [24], respectively:

$$C = \frac{4I \times \Delta t}{m \times \Delta V} \quad (1)$$

$$E = \frac{C\Delta V^2}{8} \quad (2)$$

$$P = \frac{\Delta V^2}{4R_{ESRm}} \quad (3)$$

where C = specific capacitance (F g^{-1}), t = discharge time, I = applied current density, ΔV = voltage drop of discharging curve, m = total mass of both electrodes, E = specific energy (Wh kg^{-1}), P = specific power (W kg^{-1}) and V = potential (Volts).

Electrochemical analysis: A Neware battery tester and an electrochemical workstation (SP-300 Biologic EC lab) and were employed to conduct cyclic voltammetry (CV), galvanostatic charge-discharge (GCD) and long-term stability evaluations of the supercapacitors. All experiments were carried out utilizing a 2-electrode cell system. CV tests were conducted at scan rates of 5, 10, 20 and 50 mV s^{-1}, while GCD experiments were performed at current densities ranging from 1 to 20 A g^{-1}. The experiments utilized 6 M KOH as an aqueous electrolyte and 1 M $TEABF_4$ in acetonitrile as a non-aqueous electrolyte. Methods for GCD were employed in performing long-term stability assessments at current densities of 1 A and 5 A g^{-1}.

RESULTS AND DISCUSSION

Structural studies: The X-ray diffraction (XRD) patterns of TRAC 800 and TRAC 900, as shown in Fig. 1, reveal distinct diffraction peaks at 23.2º and 44.3º. These peaks correspond to the (002) and (100) planes of disordered carbon, as identified by the Joint Committee on Powder Diffraction Standards (JCPDS) file No. 41-1487. The absence of any additional peaks suggests that the acid-washing process effectively eliminates residual impurities or unwanted phases, ensuring high-purity carbon materials. The difference in peak intensity between TRAC 800 and TRAC 900 indicates a variation in the degree of graphitization. At higher carbonization temperatures, such as in TRAC 900, the increased thermal energy facilitates the reorganization of carbon atoms into a more ordered, graphitic structure. This transition reduces the proportion of amorphous carbon and enhances the material's electrical conductivity [25]. The higher graphitic nature of TRAC 900, compared to TRAC 800, suggests that elevated temperatures promote the growth of larger and more ordered graphitic domains, improving electron mobility and overall conductivity [26].

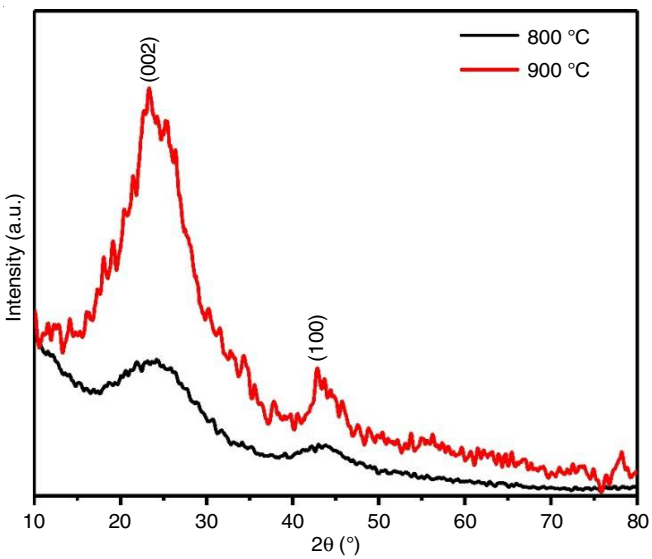

Fig. 1. XRD pattern of TRAC 800 and TRAC 900

Moreover, the porous nature of the carbon materials plays a critical role in their electrochemical performance. Higher carbonization temperatures often lead to the development of a well-defined porous network by volatilizing non-carbon elements and increasing the structural stability of carbon framework. This porous architecture enhances the surface area, which is crucial for charge storage applications, as it facilitates ion diffusion and improves electrolyte accessibility. Therefore, the combined effects of increased graphitization and optimized porosity at higher temperatures contribute to superior charge storage capacity and better electrochemical performance of TRAC 900 compared to TRAC 800.

Raman studies: The Raman spectra of TRAC 800 and TRAC 900 (Fig. 2) highlighted the structural variations in these carbon-based materials. Two prominent peaks at 1329 cm^{-1} (D-band) and 1592 cm^{-1} (G-band) correspond to disorder and graphitic order, respectively. The G-band arises from sp^2 carbon stretching in a hexagonal arrangement, whereas the D-band signifies structural defects and amorphous carbon. The I_D/I_G ratio serves as a measure of disorder, with a lower ratio indicating greater graphitization. TRAC 800 exhibits a higher I_D/I_G ratio (~1.10), suggesting increased disorder, while TRAC 900 has a lower ratio (~0.85), reflecting enhanced structural organization [27]. The sharper peaks observed in TRAC 900 further support its improved carbon ordering. Furthermore, a well-defined 2D peak at ~2700 cm^{-1} appears in TRAC 900, signifying a more graphitic structure with fewer layers. In contrast, TRAC 800 lacks this peak, indicating a less ordered graphene structure. This variation underscores the impact of temperature on the structural evolution. The reduction in the I_D/I_G ratio from TRAC 800 to TRAC 900 underscores the influence of increased temperatures on atomic mobility and the acceleration of graphitization. This structural refinement is essential for applications requiring high carbon order, demonstrating the significant role of thermal treatment in modifying carbon properties.

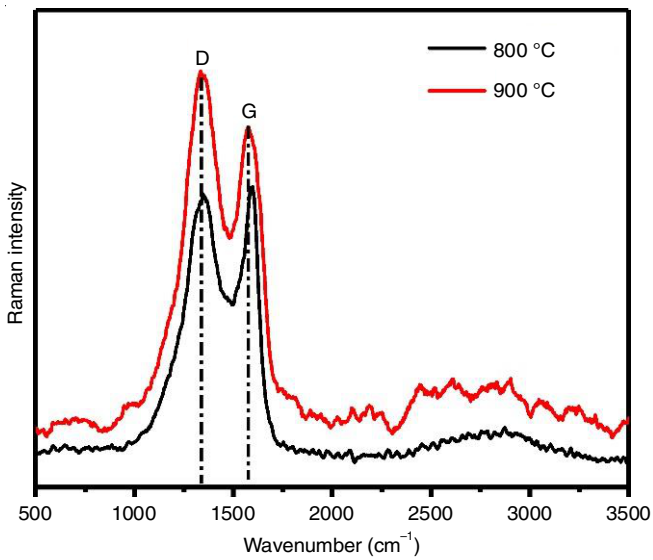

Fig. 2. Raman of TRAC 800 and TRAC 900

BET studies: The BJH (Barrett-Joyner-Halenda) pore size distribution analysis (Fig. 3a) of TRAC 800 and TRAC 900 confirms the presence of both micropores and mesopores, essential for effective charge storage. TRAC 900 exhibits a more uniform pore size distribution compared to TRAC 800, indicating an improved porous structure due to higher activation temperature.

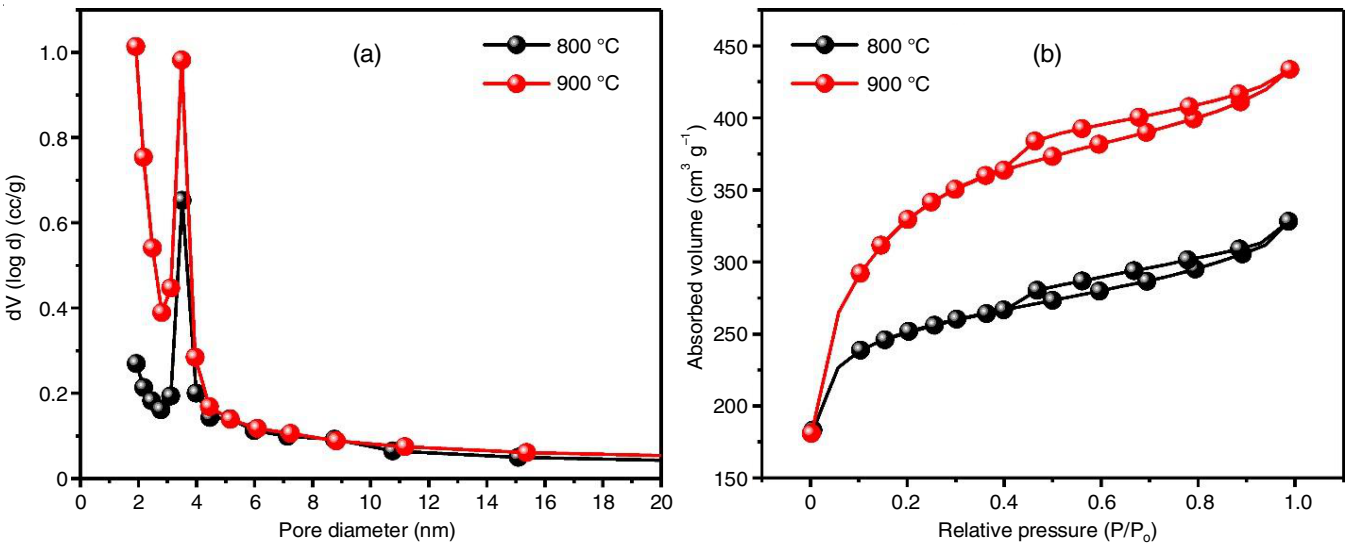

Fig. 3. (a) BJH pore size distribution of TRAC 800 and TRAC 900 and (b) N_2 adsorption/desorption isotherms of TRAC 800 and TRAC 900

The average pore size of TRAC 800 is 0.81 nm, while TRAC 900 has an average pore size of 0.93 nm. The total pore volume for TRAC 800 and TRAC 900 is 0.016 and 0.038 $cm^3 g^{-1}$, respectively. The increased pore volume and optimized pore structure in TRAC 900 enhance electrolyte penetration and ion transport, leading to superior electrochemical performance for supercapacitor applications [28]. Fig 3b showed H3-type hysteresis revealing the slit-shaped pores and type IV isotherm with the surface area about 940.14 $m^2 g^{-1}$ with the average pore volume of 0.016 $cm^3 g^{-1}$, with a pore size distribution primarily in the 0.81 nm range, suggesting the presence of micropores and small mesopores. At increased activation temperature 900 ºC, the hysteresis and isotherm of TRAC 900 are slightly modified and its surface area is enhanced to1158.06 $m^2 g^{-1}$. Also, the pore volume increases to 0.038 $cm^3 g^{-1}$, while the pore size distribution shifts towards a broader range of 0.93 nm, indicating a greater presence of mesopores. This shift suggests that the higher activation temperature facilitates the formation of both micropores and mesopores due to enhanced gasification, improving ion transport pathways.

Surface morphological studies: The surface morphology of the obtained TRAC 800 and TRAC 900 samples was analyzed using SEM. Fig. 4a-b display the SEM images of TRAC activated at 800 ºC, revealing a highly agglomerated surface with irregularly connected pores. Under N_2 atmosphere activation, the surface exhibited significant roughness, but the pores were not distinctly visible, suggesting incomplete pore development at this temperature. In contrast, at 900 ºC activation (Fig. 4c-d), a more uneven surface with wider and better-defined pores was observed, indicating a noticeable increase in porosity and surface area.

The pore volume and pore size distribution play a crucial role in determining the electrochemical performance of the material. The BET analysis reveals that TRAC 800 exhibits a pore volume of 0.016 cm^3/g, with a pore size distribution primarily in the 0.81 nm range, suggesting the presence of micropores and small mesopores. At 900 ºC, the pore volume increases to 0.038 cm^3/g, while the pore size distribution shifts towards

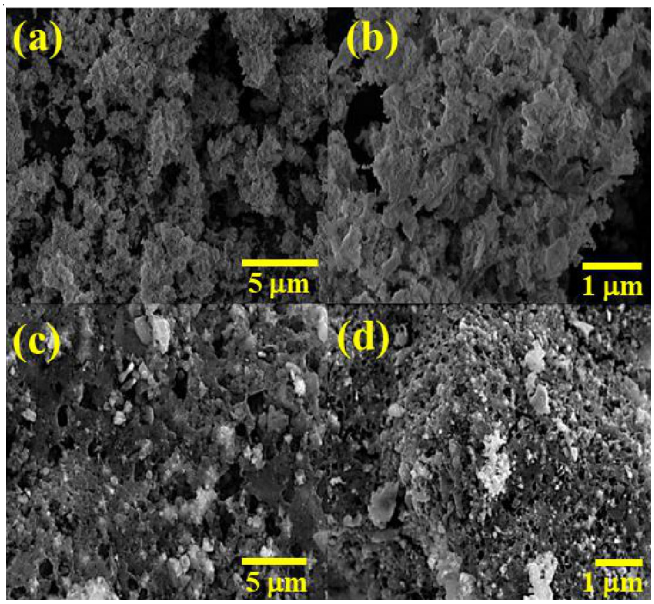

Fig. 4. FE-SEM images of TRAC 800 (a&b) and TRAC 900 (c&d)

a broader range of 0.93 nm, indicating a greater presence of mesopores. This shift suggests that the higher activation temperature facilitates the formation of both micropores and mesopores due to enhanced gasification, improving ion transport pathways [29]. The increased pore volume and optimized pore size distribution at 900 ºC significantly enhance the accessibility of electrolyte ions, thereby improving charge storage capacity and electrochemical performance. The interconnected porous network enables efficient ion diffusion, reduces internal resistance and enhances the rate capability of material, making it highly suitable for supercapacitor applications [30]. Based on the optimum results of XRD, Raman, BET and FE-SEM, TRAC 900 was opted for further electrochemical analysis.

Electrochemical characterization: Using cyclic voltammetry (CV) and galvanostatic charge-discharge (GCD) methodologies, the capacitive performance of the samples was evaluated in both aqueous (KOH) and non-aqueous ($TEABF_4$) electro-

lytes, with working potential windows of 0-0.9 V and 0-2.7 V, respectively. Fig. 5 presents the CV profiles of symmetrical supercapacitors at various scan rates (5, 10, 20 and 50 mV s^{-1}) across a broad voltage range for each sample. At lower scan rates (5 and 10 mV s^{-1}), the CV curves exhibit a nearly ideal rectangular shape, indicating excellent double-layer capacitive behaviour with minimal resistive losses. As the scan rate increases to 20 and 50 mV s^{-1}, the rectangular shape remains well-preserved, suggesting good charge propagation and efficient ion diffusion within the hierarchical pore structure. The absence of distinct redox peaks further confirms the dominance of electric double-layer capacitance (EDLC) behaviour over faradaic reactions in these samples.

As the scan rate increases, the CV curves maintain their rectangular nature but exhibit a slight distortion due to increased internal resistance. This behaviour is characteristic of high performance supercapacitors, where a well-maintained rectangular shape at higher scan rates indicates fast ion transport and excellent capacitive response, even at higher current densities. The ability of the electrode material to sustain its capacitive performance under increasing scan rates highlights its potential for high-power applications, where rapid charge/discharge cycles are essential. This behaviour is attributed to the well-developed porous structure, which facilitates rapid electrolyte ion movement and reduces diffusion resistance. The interconnected network of micropores and mesopores ensures efficient charge storage, enabling the material to deliver high capacitance with excellent rate capability [31].

Rate capability is another important consideration when evaluating the performance of the capacitive electrode in power applications. An appropriate electrode is required to give a high specific capacitance at a high charge discharge rate. Furthermore, galvanostatic charge-discharge (GCD) research was conducted using the same potential window as the CV experiment [32]. The GCD profiles of TRAC 900 with aqueous and non-aqueous electrolytes at different current densities (1 to 10 Ag^{-1}) are displayed in Fig. 6a-b. The GCD curves maintain regular triangular shapes throughout all current rates, indicating that they have low internal resistances due to their huge specific surface area and extensively ordered porous nature.

The electrochemical performance of TRAC 900 was evaluated in both aqueous (6 M KOH) and non-aqueous ($TEABF_4$) electrolytes to assess their suitability for high-performance supercapacitors. The mass-specific capacitances of TRAC 900 were measured as 66.27 F g^{-1} at 3 A g^{-1} in non-aqueous mode, increasing to 156.02 F g^{-1} at the same current density in aqueous mode. This enhancement in aqueous conditions can be attributed to the superior ionic conductivity nature of KOH and broader electrochemical stability window of $TEABF_4$, which contributed to an ~42-56% increase in capacitance [33]. TRAC 900 exhibited superior electrochemical performance primarily due to its higher micropore content. Since capacitance is largely derived from micropores, lower micropore density will restrict ion-accessibility and storage capacity. This limitation arises because electrolyte ions require adequate time to penetrate the carbon matrix, which is less efficient in materials with fewer micropores. In contrast, the well-optimized pore structure of TRAC 900 enhances electrolyte penetration and ion diffusion, leading to improved charge storage performance.

Further the extent of the practical application, the cyclic stability of TRAC 900 electrode was analyzed, which keeps above 99% for entire 13,000 cycles (Fig 7a), further revealing the high reversibility in both aqueous and non-aqueous mode. To further assess the energy storage performance of the supercapacitor device, the energy density is determined by using eqn. 2 and the power density can be analyzed by eqn. 3. In consequence, the Ragone plot of E *vs*. P is supplied in Fig. 7b. The resultant values reach about 12.99 at 10 A g^{-1} and 105263.15 W kg^{-1}. These findings confirm the superior capacitive behaviour of TRAC 900, particularly in non-aqueous electrolytes. The capacitive performance in aqueous mode is primarily governed by rapid ion diffusion and efficient electrolyte accessibility.

The specific capacitance of TRAC 900 was further analyzed across varying current densities. In aqueous mode, it achieved capacitance values 241.13 F g^{-1} at 1 A g^{-1}, 217.49 F g^{-1} at 2 A g^{-1}, 156.02 at 3 A g^{-1}, 106.38 at 5 A g^{-1}, 118. 20 F g^{-1} at 10 A

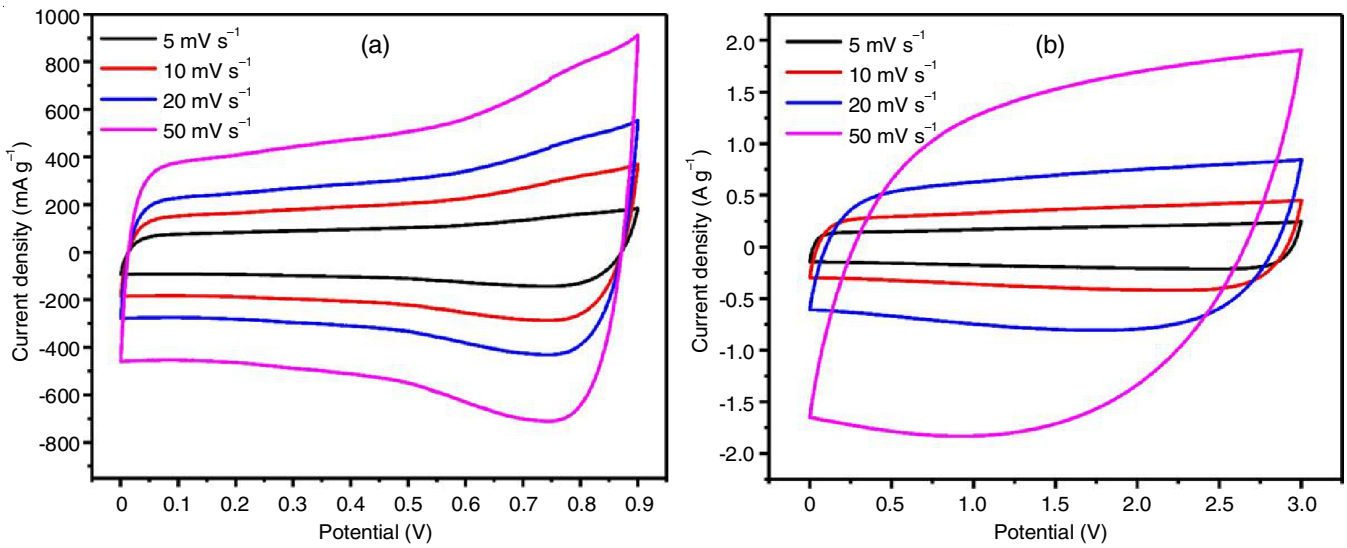

Fig. 5. Cyclic voltammograms of TRAC 900 in (a) In 6 M KOH (b) $TEABF_4$ electrolyte

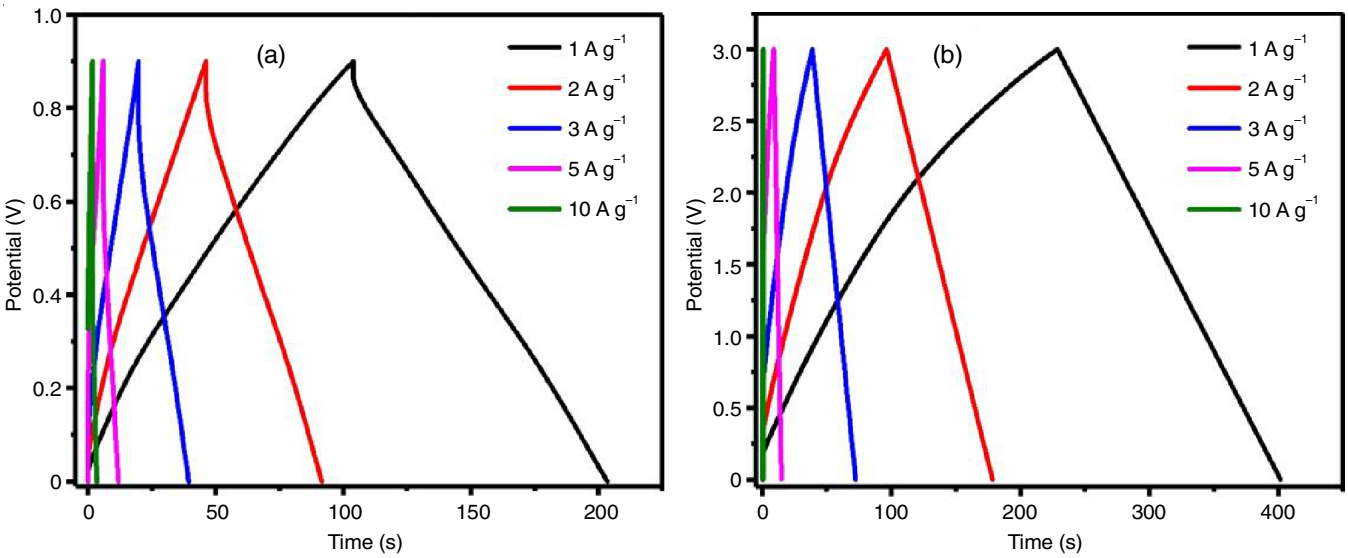

Fig. 6. Galvanostatic charge-discharge profiles of TRAC 900 in 6 M (a) KOH (b) $TEABF_4$ electrolyte

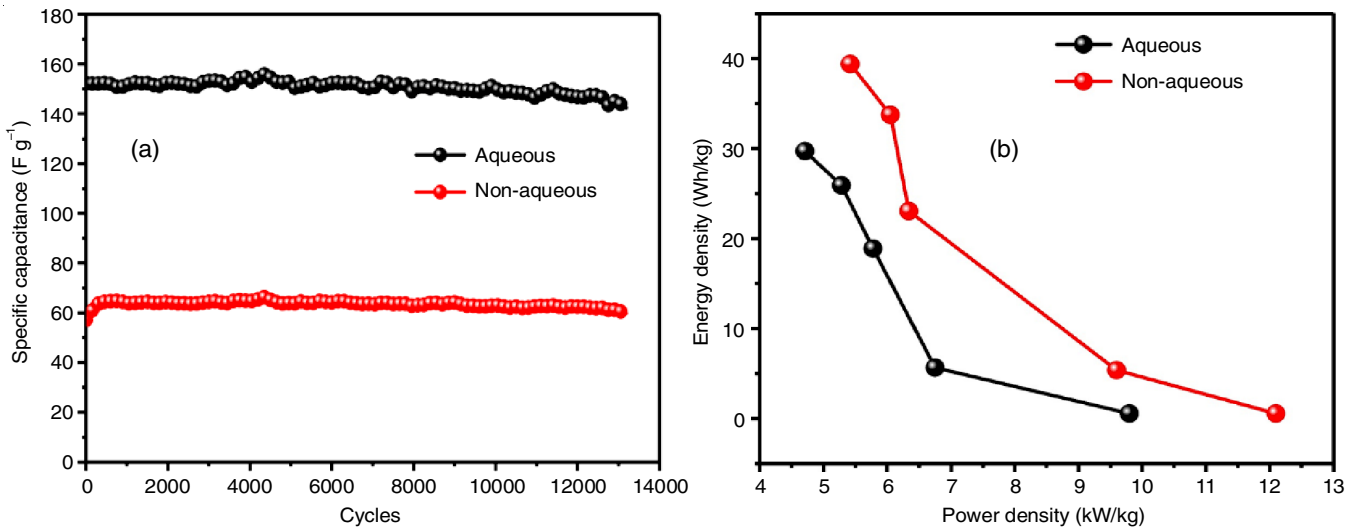

Fig. 7. (a) Cyclic stability for the electrode TRAC 900 in $TEABF_4$ and (b) Ragone plots for the electrode TRAC 900 in KOH and $TEABF_4$

g^{-1}. The corresponding energy densities reached 97.65 Wh kg^{-1}, 88.08 Wh kg^{-1}, 63.19 Wh kg^{-1}, 43.08 Wh kg^{-1} and 47.87 Wh kg^{-1}, respectively. Their respective power densities were 3446.80 W kg^{-1}, 6893.61 W kg^{-1}, 10340.42 W kg^{-1}, 17234.04 W kg^{-1} and 34468. 08 W kg^{-1}. In non-aqueous $TEABF_4$ electrolyte, TRAC 900 exhibited even higher capacitance values of 112.41 at 1 A g^{-1}, 106.56 at 2 A g^{-1}, 66.27 at 3 A g^{-1} 19.49 at 5 A g^{-1} and 12.99 at 10 A g^{-1}. The corresponding energy densities reached 505.84 Wh kg^{-1}, 479.53 Wh kg^{-1}, 298.24 Wh kg^{-1}, 87.71 Wh kg^{-1} and 58.47 Wh kg^{-1}, respectively. Their respective power densities were 10526.31 W kg^{-1}, 21052.63 W kg^{-1}, 31578.94 W kg^{-1}, 52631.57 W kg^{-1} and 105263.15 W kg^{-1}. These findings confirm the superior capacitive behaviour of TRAC 900, particularly in non-aqueous electrolytes. The capacitive performance in aqueous mode is primarily governed by rapid ion diffusion and efficient electrolyte accessibility.

However, a decrease of ~42-56 % in specific capacitance was observed at higher current densities due to the limited voltage window and lower ionic conductivity of KOH. This trend emphasizes the influence of electrolyte composition on charge storage efficiency, with $TEABF_4$ providing superior stability under high current loads. Despite some capacitance reduction at higher current densities, TRAC 900 exhibited excellent capacitance retention, highlighting its ability to sustain rapid charge-discharge cycles with minimal performance degradation. The combination of a well-optimized pore structure, high surface area and enhanced ion transport further supports its potential as an efficient electrode material for high-energy-density supercapacitor applications.

Conclusion

This study successfully demonstrates the transformation of waste tea residues into high-performance supercapacitor electrode materials through a single-step activation process in an N_2 atmosphere using $ZnCl_2$ at two different temperatures. The activation at 900 ºC significantly enhances the specific surface area (1158.06 m^2/g), facilitating efficient electrolyte diffusion and improving the double-layer capacitive perfor-

mance. The optimized porous structure of the synthesized materials enables superior charge storage and ion transport, resulting in excellent electrochemical performance. TRAC 900 exhibited remarkable capacitive behaviour in aqueous (KOH) and non-aqueous ($TEABF_4$) electrolytes. Notably, TRAC 900 demonstrated high power density in non-aqueous conditions, achieving a specific capacitance of 112.41 at 1 A g^{-1}, 106.56 at 2 A g^{-1}, 66.27 at 3 A g^{-1}, 19.49 at 5 A g^{-1} and 12.99 at 10 A g^{-1}. The corresponding energy densities reached 505.84 Wh kg^{-1}, 479.53 Wh kg^{-1}, 298.24 Wh kg^{-1}, 87.71 Wh kg^{-1} and 58.47 Wh kg^{-1}, respectively. Their respective power densities were 10526.31 W kg^{-1}, 21052.63 W kg^{-1}, 31578.94 W kg^{-1}, 52631.57 W kg^{-1} and 105263.15 W kg^{-1}. At non-aqueous conditions, TRAC 900 exhibited high energy density achieving an exceptional specific capacitance of 112.41 F g^{-1} at 1 A g^{-1} and excellent cycling stability retaining 96.66% of its capacitance after 16,000 cycles. A maximum energy density of 505.84 Wh kg^{-1} was achieved at 1 A g^{-1} with a corresponding power density of 10,526.31 W kg^{-1} highlighting its superior energy storage capability in non-aqueous electrolytes. These results validate the feasibility of utilizing porous carbon derived from tea residue as a sustainable and cost-effective electrode material for next-generation supercapacitors. The study also provides a scalable approach for biomass-derived carbon materials, paving the way for large-scale production of high energy-density supercapacitors.

ACKNOWLEDGEMENTS

The authors gratefully acknowledge the support provided by Vels Institute of Science, Technology & Advanced Studies (VISTAS), Chennai, India. The authors also extend their sincere gratitude to the Sophisticated Analytical Instrument Facility (SAIF), IIT Madras, Chennai, and Pondicherry University, Pondicherry, for their assistance in material characterization.

CONFLICT OF INTEREST

The authors declare that there is no conflict of interests regarding the publication of this article.

REFERENCES

1. M. Winter and R.J. Brodd, *Chem. Rev.*, **104**, 4245 (2004); https://doi.org/10.1021/cr020730k
2. S. Ghosh, R. Santhosh, S. Jeniffer, V. Raghavan, G. Jacob, K. Nanaji, P. Kollu, S.K. Jeong and A.N. Grace, *Sci. Rep.*, **9**, 16315 (2019); https://doi.org/10.1038/s41598-019-52006-x
3. S. Saini, P. Chand and A. Joshi, *J. Energy Storage*, **39**, 102646 (2021); https://doi.org/10.1016/j.est.2021.102646
4. M. Alzaid, F. Alsalh and M.Z. Iqbal, *J. Energy Storage*, **40**, 102751 (2021); https://doi.org/10.1016/j.est.2021.102751
5. E. Taer, M. Melisa, A. Agustino, R. Taslim, W.S. Mustika and A. Apriwandi, *Energy Sources A Recovery Util. Environ. Effects*, **47**, 9490 (2021); https://doi.org/10.1080/15567036.2021.1950871
6. D. Chen, L. Yang, J. Li and Q. Wu, *ChemistrySelect*, **4**, 1586 (2019); https://doi.org/10.1002/slct.201803413
7. S.J. Rajasekaran, A.N. Grace, G. Jacob, A. Alodhayb, S. Pandiaraj and V. Raghavan, *Catalysts*, **13**, 286 (2023); https://doi.org/10.3390/catal13020286
8. L. Sinha and P.M. Shirage, *J. Electrochem. Soc.*, **166**, A3496 (2019); https://doi.org/10.1149/2.1251914jes
9. Y. Song, W. Qu, Y. He, H. Yang, M. Du, A. Wang, Q. Yang and Y. Chen, *J. Energy Storage*, **32**, 101877 (2020); https://doi.org/10.1016/j.est.2020.101877
10. R. Vinodh, C.V.V.M. Gopi, V.G.R. Kummara, R. Atchudan, T. Ahamad, S. Sambasivam, M. Yi, I.M. Obaidat and H.-J. Kim, *J. Energy Storage*, **32**, 101831 (2020); https://doi.org/10.1016/j.est.2020.101831
11. A. Shokry, M. Karim, M. Khalil, S. Ebrahim and J. El Nady, *Sci. Rep.*, **12**, 11278 (2022); https://doi.org/10.1038/s41598-022-15477-z
12. Z. Ren, H. Luo, H. Mao, A. Li, R. Dong, S. Liu and Y. Liu, *Chem. Phys. Lett.*, **760**, 138019 (2020); https://doi.org/10.1016/j.cplett.2020.138019
13. T. Giannakopoulou, N. Todorova, A. Erotokritaki, N. Plakantonaki, A. Tsetsekou and C. Trapalis, *Appl. Surf. Sci.*, **528**, 146801 (2020); https://doi.org/10.1016/j.apsusc.2020.146801
14. L. Zhang, X. Yu, P. Zhu, R. Sun and C. Wong, *J. Electroanal. Chem.*, **876**, 114478 (2020); https://doi.org/10.1016/j.jelechem.2020.114478
15. Y. Gao, S. Zheng, H. Fu, J. Ma, X. Xu, L. Guan, H. Wu and Z.-S. Wu, *Carbon*, **168**, 701 (2020); https://doi.org/10.1016/j.carbon.2020.06.063
16. N. Cai, H. Cheng, H. Jin, H. Liu, P. Zhang and M. Wang, *J. Electroanal. Chem.*, **861**, 113933 (2020); https://doi.org/10.1016/j.jelechem.2020.113933
17. C. Wang, D. Wu, H. Wang, Z. Gao, F. Xu and K. Jiang, *J. Colloid Interface Sci.*, **523**, 133 (2018); https://doi.org/10.1016/j.jcis.2018.03.009
18. D.R. Lobato-Peralta, E. Duque-Brito, H.O. Orugba, D.M. Arias, A.K. Cuentas-Gallegos, J.A. Okolie and P.U. Okoye, *Diamond Rel. Mater.*, **138**, 110176 (2023); https://doi.org/10.1016/j.diamond.2023.110176
19. Y. Zhang, Z. Gao, N. Song and X. Li, *Electrochim. Acta*, **222**, 1257 (2016); https://doi.org/10.1016/j.electacta.2016.11.099
20. Z. Qin, Y. Ye, D. Zhang, J. He, J. Zhou and J. Cai, *ACS Omega*, **8**, 5088 (2023); https://doi.org/10.1021/acsomega.2c07932
21. A. Bello, N. Manyala, F. Barzegar, A.A. Khaleed, D.Y. Momodu and J.K. Dangbegnon, *RSC Adv.*, **6**, 1800 (2016); https://doi.org/10.1039/C5RA21708C
22. T.G. Çakmak, B. Saricaoglu, G. Ozkan, M. Tomas and E. Capanoglu, *Food Sci. Nutr.*, **12**, 3112 (2024); https://doi.org/10.1002/fsn3.4011
23. B. Li, J. Hu, H. Xiong and Y. Xiao, *ACS Omega*, **5**, 9398 (2020); https://doi.org/10.1021/acsomega.0c00461
24. A. Khan, R.A. Senthil, J. Pan, S. Osman, Y. Sun and X. Shu, *Electrochim. Acta*, **335**, 135588 (2020); https://doi.org/10.1016/j.electacta.2019.135588
25. H. Zhao, H. Zhong, Y. Jiang, H. Li, P. Tang, D. Li and Y. Feng, *Materials*, **15**, 895 (2022); https://doi.org/10.3390/ma15030895
26. X.B. Xie, D. Wu, H. Wu, C. Hou, X. Sun, Y. Zhang, R. Yu, S. Zhang, B. Wang and W. Du, *J. Mater. Sci. Mater. Electron.*, **31**, 18077 (2020); https://doi.org/10.1007/s10854-020-04358-8
27. Y. Yan, S. Manickam, E. Lester, T. Wu and C.H. Pang, *Ultrason. Sonochem.*, **73**, 105519 (2021); https://doi.org/10.1016/j.ultsonch.2021.105519
28. A. Derylo-Marczewska, K. Skrzypczyñska, K. Kusmierek, A. Swiatkowski and M. Zienkiewicz-Strzalka, *Adsorption*, **25**, 357 (2019); https://doi.org/10.1007/s10450-019-00016-6
29. M. Danish, T. Ahmad, R. Hashim, N. Said, M.N. Akhtar, J. Mohamad-Saleh and O. Sulaiman, *Surf. Interfaces*, **11**, 1 (2018); https://doi.org/10.1016/j.surfin.2018.02.001
30. H. Du, Y. Yang, C. Zhang, Y. Li, J. Wang, K. Zhao, C. Lu, D. Sun, C. Lu, S. Chen and X. Ma, *J. Power Sources*, **614**, 234988 (2024); https://doi.org/10.1016/j.jpowsour.2024.234988
31. Q. Wang, B. Luo, Z. Wang, Y. Hu and M. Du, *Molecules*, **29**, 5172 (2024); https://doi.org/10.3390/molecules29215172
32. Y. Li, Q. Liu, Q. Zhang, X. Li, Y. Yang, P. Wang, K. Li, Y. Li, F. Zhong, Q. Liu, Y. Zheng, X. Yang and P. Zhao, *Green Chem.*, **26**, 12019 (2024); https://doi.org/10.1039/D4GC04103H
33. T.K. Ghosh, D.L. Singh and G.R. Rao, *Electrochim. Acta*, **500**, 144752 (2024); https://doi.org/10.1016/j.electacta.2024.144752